Int. J. Electrochem. Sci., 15 **(2020)** 9473 – 9486, doi: 10.20964/2020.09.59

International Journal of
ELECTROCHEMICAL
SCIENCE
www.electrochemsci.org

Effects of Silver Modification of $La_{0.8}Sr_{0.2}MnO_{3-\delta}$ Cathode on the Catalytic Activity for the Oxygen Reduction Reaction in a Flexible Al-Air Battery

Changjing Fu[2], *Qiang Ma*[1,*], *Qibing Wu*[3], *Zaifang Yuan*[3], *Jun He*[1]

[1] School of Instrumentation Science and Engineering, Harbin Institute of Technology, Harbin 150001, China
[2] School of Materials Science and Engineering, Heilongjiang University of Science &Technology, Harbin 150022, China
[3] State Key Laboratory of Advanced Chemical Power Sources, Guizhou Meiling Power Sources Co. Ltd, Zunyi, Guizhou 563003, China
[*]E-mail: qiangma@hit.edu.cn

Received: 10 April 2020 / *Accepted:* 25 June 2020 / *Published:* 10 August 2020

An additive-free 3D hierarchical air electrode, consisting of silver-decorated perovskite oxide $La_{0.8}Sr_{0.2}MnO_{3-\delta}$ (LSM)/carbon fiber cloth (CFC), was designed and synthesized by a hydrothermal-calcination route. The surface chemistries and microstructures of Ag/LSM/CFC were characterized, and its bifunctional electrocatalysis effects were examined in this article. The results showed that the catalytic activity of LSM/CFC toward the oxygen reduction reaction (ORR) was greatly improved by the silver modification. The superior 3D hierarchical electrode microstructure and the good interface between the silver and LSM resulted in a large electrochemical active area and more catalytic sites. Ag/LSM/CFC exhibited a high half-wave potential of 0.833 V, a small Tafel slope of 48.81 $mV \cdot dec^{-1}$ and a large electrochemical surface area (C_{dl}=82.16 $mF \cdot cm^{-2}$) in 0.1 M KOH solution at room temperature. Furthermore, a flexible Al-air battery with this kind of 3D hierarchical air electrode delivered a high power density of 5.14 $mW \cdot cm^{-2}$ and excellent stability.

Keywords: $La_{0.8}Sr_{0.2}MnO_{3-\delta}$ (LSM), Silver, 3D hierarchical air electrode, Oxygen reduction reaction (ORR), Al-air battery

1. INTRODUCTION

With the fast depletion of fossil fuels and the increasing environmental pollution, the search for novel and alternative energy resources has been a high priority [1]. Al-air batteries have aroused research interest due to their high energy densities and long operational lives [2]. Especially in recent years, to meet the development requirements of bendable and wearable electronic products, research on flexible

supercapacitors and batteries and other wearable energy storage and conversion devices has become a top priority [3]. It is required that the novel and alternative energy device should exhibit good electrochemical performance, be easily used by humans, and have the characteristics of deformability, light weight and low cost [4-6].The flexible Al-air battery has thus stimulated interest due to the inertness of its material, ease of handling in an ambient environment, a high volumetric capacity, low price, abundance of resources, non-toxicity and environmental friendliness [7, 8]. However, there are still some puzzles that are difficult to resolve, which impede the commercialization of Al-air batteries. Among them, the major bottleneck is the sluggish oxygen reduction reaction (ORR) kinetics in air cathodes [9]. Therefore, the development of efficient and stable electrocatalysts that can significantly reduce the large cathode overpotentials for ORR has currently become a hot research topic with Al-air batteries.

Recent studies on the electrocatalysts of oxygen electrode materials are focused on Pt and its alloys, carbon materials, transition metal oxides, perovskite oxides, and their compounds [10]. Although platinum and other precious metals have excellent catalytic activity, their practical application is limited by the degradation of catalyst stability, which is caused by the surface oxidation and dissolution of metals in the process of the ORR; additionally, they are expensive [11-13]. Perovskite oxides have been widely studied and applied as a cathode material for solid oxide fuel cells due to its excellent chemical stability and high electron conductivity at high temperature (≥ 1073 K) [14]. Recently, perovskite oxides are considered to be a possible electrocatalyst to replace Pt-based catalysts because of their unique crystal structure [11, 15]. Theoretical calculations confirm that among them, $LaMnO_3$ has superior electrocatalytic activity toward the ORR [16, 17]. In particular, Sr doping in the A site of $LaMnO_3$ can adjust its band structure and the valence of Mn [18-20], thus significantly enhancing the surface absorbance of oxygen and its electrocatalytic activity [21-23]. However, to the best of our knowledge, the reported electrocatalytic activity of $La_{1-x}Sr_xMnO_3$ toward the ORR is still less than that of Pt-based precious metals in an alkaline solution; therefore, only a handful of investigators have paid attention to the research of perovskite oxides as low-temperature electrocatalysts [24]. Silver has also been identified as a promising ORR catalyst because of its low cost and high stability. Unfortunately, the relatively low catalytic activity toward the ORR of silver in alkaline solutions inhibits its application in a real battery [25-27]. Based on DFT calculations, Qaseem et al [28] designed various nanoalloys, such as Ag-Cu and Ag-Au to improve the electrocatalytic performance of silver. Xue et al [29] modified $LaMnO_3$ with silver doped in the A site to adjust its catalytic mechanism. However, to the best of our knowledge, research on silver-decorated $LaMnO_3$ perovskite oxides as ORR electrocatalysts has not yet been reported.

In this article, an additive-free and three-dimensional (3D) hierarchical air electrode is designed by constructing a silver-decorated $La_{0.8}Sr_{0.2}MnO_{3-\delta}$ (LSM) on a flexible carbon fiber cloth (CFC) substrate. The combination of CFC, LSM and Ag in one integrated electrode increases the electrical conductivity of LSM at room temperature on the one hand [30-32]; and helps to form highly conductive interconnected networks in the CFC on the other, which facilitates the absorption of electrolyte and thus accelerates the redox kinetics of the cathode. The effects of the composition and microstructure of Ag/LSM/CFC on the oxygen electrocatalysis properties are explored in depth in an alkaline solution. The discharge performance of a flexible Al-air battery with Ag/LSM/CFC as an air cathode was measured.

2. EXPERIMENTAL

2.1 Preparation of the air electrode

All chemicals used in this experiment were of analytical grade without further treatment. Carbon fiber cloth (CFC), purchased from Taiwan Carbon Energy Technology Co. LTD. (CeTech), was chosen as a flexible substrate. The CFC was cleaned before use. The cleaning steps were as follows. First, it was ultrasonically cleaned by acetone, ethanol and distilled water for 30 min, successively, and then put in a drying oven at 65 °C for approximately 6-8 h before use.

The perovskite oxide $La_{0.8}Sr_{0.2}MnO_{3-\delta}$ (LSM) was deposited on the CFC surface by the following hydrothermal synthesis method. First, 0.04 mol $La(NO_3)_3 \cdot H_2O$, 0.01 mol $Sr(NO_3)_2$ and 0.05 mol $Mn(CH_3COOH)_2 \cdot 4H_2O$ were dissolved into 50 mL distilled water to prepare a solution with a total metal ion concentration of 2 $mol \cdot L^{-1}$. Then, 0.3 mol of urea was put into it as a coprecipitator to form a brown solution. The CFC was soaked in the prepared solution for 15 min and then transferred into a stainless steel autoclave and heated at 120 °C for 24 h. After that, the CFC was sifted out of the solution, washed three times with ethanol and distilled water, successively, and then dried in vacuum at 65 °C for a few hours. Thus-prepared samples were finally calcined at 350 °C for 4 h in air, and the LSM-covered CFC was obtained and named LSM/CFC.

Ag nanoparticle-modified LSM/CFC was prepared by the following synthetic method. Silver nitrate (2 mmol) was first dissolved in 100 mL distilled water. Sodium citrate solution (14 mmol, 100 mL) was then drop wise added to the $AgNO_3$ aqueous solution under vigorous magnetic agitation. Subsequently, the mixed solution was heated at 100 °C for 30 min until it turned into a yellow emulsion. At that time, LSM/CFC was soaked in the solution for approximately 10 min. After rinsing with ethanol three times and drying in a vacuum oven at 60 °C for 3-4 h, the silver-modified LSM/CFC electrode was finally obtained and named Ag/LSM/CFC. For comparison, Ag nanoparticle-decorated CFC (Ag/CFC) was also prepared in the same way.

2.2 Physicochemical characterization

X-ray diffraction (XRD) patterns were collected on a D/max 2550-PC X-ray diffractometer by using Cu Ka radiation (λ=0.15406 nm). The scattering angles were set in a range of 10°-90° and the scanning rate was controlled at $3° \cdot min^{-1}$. The microstructure and morphology of Ag/LSM/CFC were characterized and analyzed by scanning electron microscopy (SEM, Hitachi-SU8000). The surface properties of the samples were analyzed with X-ray photoelectron spectroscopy (XPS, AXIS Ultra instrument from Kratos).

2.3 Electrochemical performance measurements

The electrocatalytic activity of the electrodes was examined in a three-electrode system on a CHI660E electrochemical workstation. In this system, a Pt sheet (1.0×1.0 cm^2) was used as the counter electrode, and a saturated calomel electrode (SCE, Hg/HgO) was chosen as the reference electrode.

Working electrodes were the abovementioned 3D hierarchical electrodes (0.5×0.5 cm^2). Cyclic voltammetry (CV) tests were performed with a scanning rate of 10-50 $mV \cdot s^{-1}$. Linear sweeping voltammetry (LSV) was conducted with a scanning rate of 5 $mV \cdot s^{-1}$. Electrochemical impedance spectroscopy (EIS) tests were carried out with a frequency ranging from 0.01 Hz to 10^5 Hz and an amplitude of 5 mV. All electrochemical tests were carried out in an oxygen-saturated alkaline solution (0.1 M KOH).

2.4 Battery assembly and testing

Flexible Al-air batteries were fabricated in a sandwich structure for power density tests. Aluminum foil (99.7% purity, 100 μm in thick) was used as the raw materials for the Al anode. An alkaline gel was used as the electrolyte and prepared by polymerizing 6 M KOH solution, acrylic acid solution and $K_2S_2O_8$ (16 wt.%). A small amount of ZnO should be added to the KOH solution as a corrosion inhibitor. An acrylic acid solution was used as the polymerization agent and was composed of acrylic acid and a cross-linker of N,N'-methylene-bisacrylamide (MBA). $K_2S_2O_8$ was the polymerization initiator. Before polymerization, the KOH solution (6 M) was first mixed with the acrylic acid solution. After that, two layers of microporous polypropylene separator (celgard 2340) were immersed in the mixture for approximately 15 min. Then, the soaked separators were removed and used to cover the cathode. Afterward, the polymerization initiator was dropped onto the separator to form a colloidal solid solution. Approximately five minutes later, an Al anode (areal density ρ=115 mg cm^{-2}) was placed on the electrolyte film, and a flexible Al-air battery was finally assembled. The assembled battery was subsequently sealed with a homemade fixture, and a working area of approximately 0.5 cm^2 was left exposed. The galvanostatic discharge testing was performed at room temperature with a multichannel Neware battery testing system (BTS-5V20mA), and the corresponding voltages were collected when stabilized. The discharge stability of the battery was measured by using chronoamperometry (CA) technique at a current density of 5 $mA \cdot cm^{-2}$.

3. RESULTS AND DISCUSSION

3.1 Microscopic morphology and structural characterization

The microstructure and morphology of Ag/LSM/CFC are shown in Figure 1. According to Figure 1a, carbon fibers are dotted by discrete spherical silver particles (2~4 μm in diameter) that form bridges between the carbon fibers. The high magnification SEM images in Figure 1b and c demonstrate that the carbon fiber surface is densely covered by LSM particles forming some small, disorderly stacked nanosheets. Nevertheless, LSM particles demonstrate a uniform surface with only some minor irregularity. The cross-section of the LSM nanosheet exhibits an orthohexagonal structure, the side length of the regular hexagon is approximately 100 nm, and the thickness of the nanosheet is close to 15 nm, as shown in Figure 1c. Figure 1d schematically illustrates the synthesis route of Ag/LSM/CFC. After the hydrothermal reaction, the hexangular LSM nanosheets exhibit a disorderly growth onto the surface

of the carbon fibers; then, silver nucleates and grows into a spherical particle on the surface of the LSM nanosheets, which helps to construct an interconnected conductive network between the carbon fibers and enlarges the active surface area of the catalyst. The formation of a good interconnected network structure is of paramount importance for catalysts obtaining smooth and stable ORR kinetics because it can guarantee the free transit of oxygen, oxygen ions and electrons at the three-phase reaction interface. Otherwise, even if the catalyst has high activity, the catalytic performance of the electrode will be very poor when under the condition of insufficient reaction areas for the three-phase reaction. Therefore, a good structural design is also necessary for obtaining a high performance cathode in addition to the activity of the catalysts.

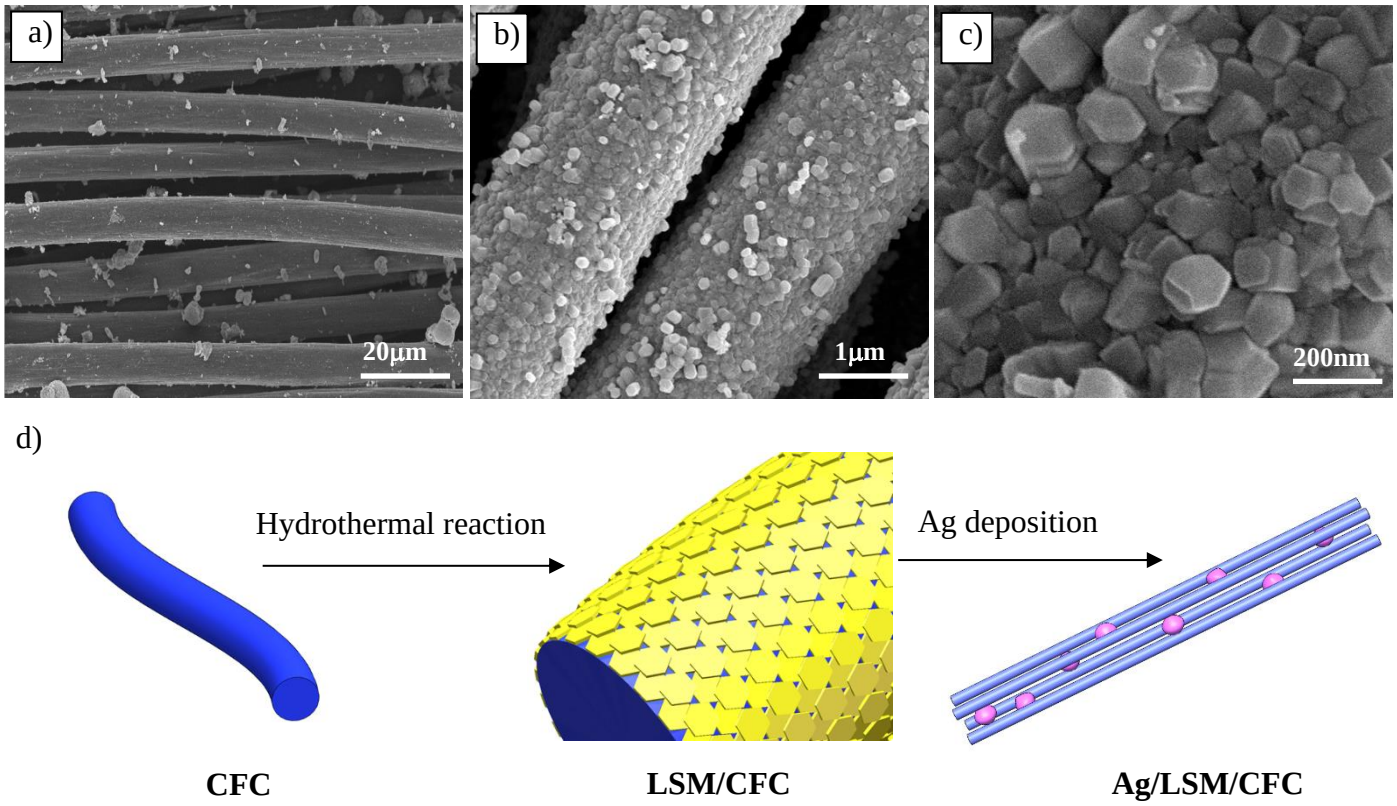

Figure 1. SEM images: (a) low-resolution SEM image of Ag/LSM/CFC, (b) low-resolution SEM image of LSM/CFC, (c) high-resolution SEM of LSM and (d) schematic illustration of the preparation process of Ag/LSM/CFC.

The XRD patterns of LSM, LSM/CFC and Ag/LSM/CFC are shown in Figure 2a. LSM peaks are observed at 2θ= 22.65°, 31.48°, 32.1°, 43.18°, 46.4°, 52.88° and 56.21°, corresponding to the (012), (110), (104), (006), (024), (122) and (214) planes, respectively, which is close to the JCPDS No. 53-0058 standard for LSM perovskite oxide (R-3c). A broadened carbon peak appears at approximately 2θ=25.8° in accordance with the (002) plane of CFC (JCPDS No.26-1083).

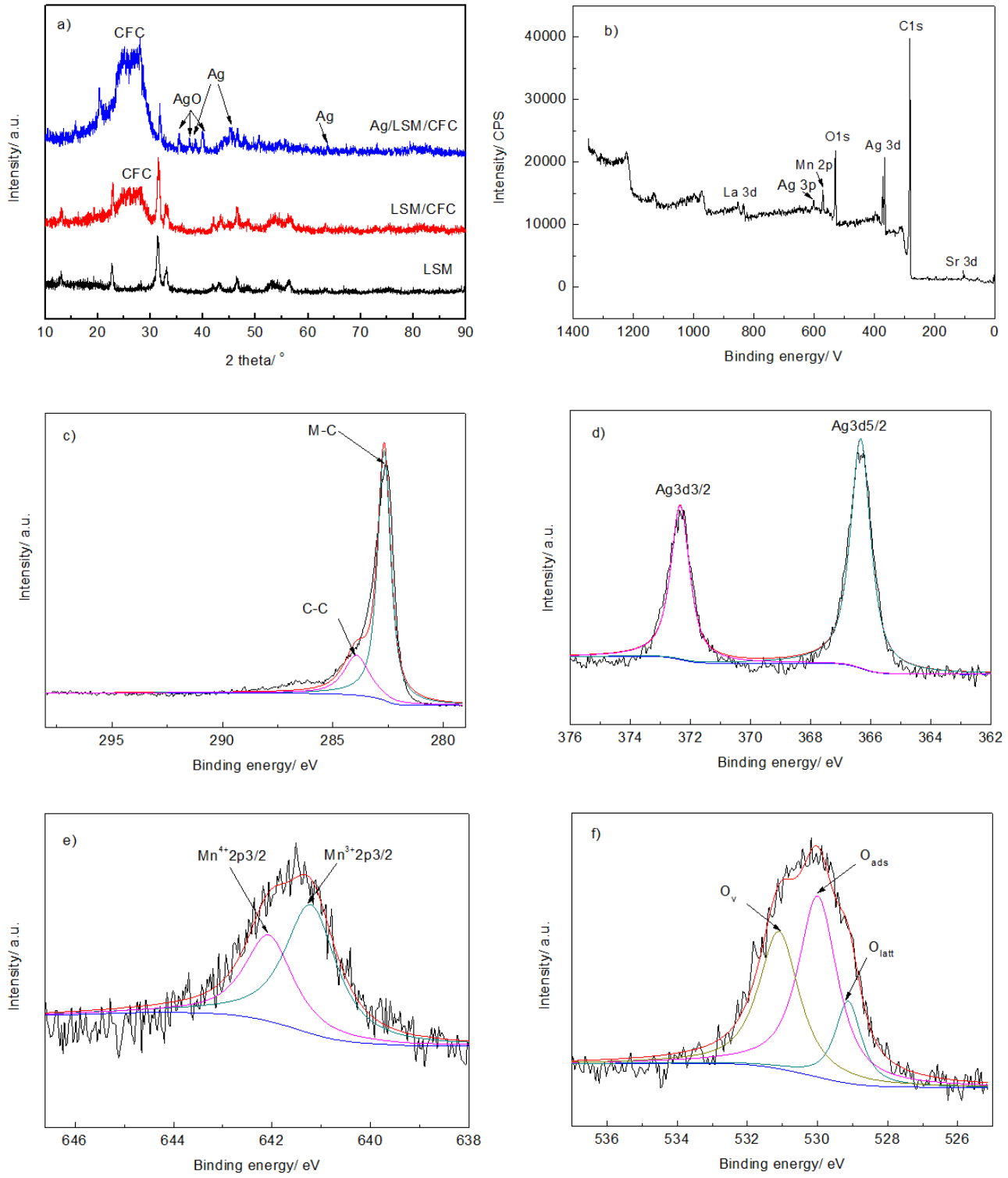

Figure 2. X-ray diffraction (XRD) patterns of the prepared catalysts (a), XPS survey scan (b), high resolution XPS spectra of C 1s (c), high resolution XPS spectra of Ag 3d (d), high resolution XPS spectra of Mn 2p (e), and high resolution XPS spectra of O 1s (f) for Ag/LSM/CFC.

Silver exists as the cubic structured silver (JCPDS No. 04-0783) and silver oxide (JCPDS No. 14-0646) in Ag/LSM/CFC suggesting that the prepared silver was oxidized to some extent during storage

and use of the samples. Besides, it can be seen from the XRD patterns that both Ag/LSM/CFC and LSM/CFC possess a pure perovskite phase of LSM, although the crystallinity is low.

Table 1. Elements contents for Ag/LSM/CFC

Elements	C1s	Ag3d	O1s	La3d	Mn2p	Sr3d
Atomic%	42.64	18.77	17.57	11.38	6	3.64

Figure 2b shows the full XPS spectrum of Ag/LSM/CFC, which confirms the existence of six elements, Ag, C, La, Sr, Mn and O, on the surface of Ag/LSM/CFC. Table 1 presents the elemental content of Ag/LSM/CFC, and several aspects of the surface properties can also be revealed. The atomic ratio of Mn/(La+Sr) is 0.4, suggesting that the surface of LSM is rich in the A-site, which is consistent with a report by Symianakis et al regarding $LaMnO_3$ perovskites [33, 34]. Moreover, it can be inferred that the preferred A-site cation is Sr as the atomic ratio of Sr/La is 0.32, which will enhance the electronic conductivity of LSM to a certain degree. In addition, the atomic ratio of O/(La+Sr+Mn) should be close to 1.5 based on electroneutrality, whereas it is only 0.836, revealing that a high valence cation (Mn^{4+}) is populated on the surface of Ag/LSM/CFC. The results of the full XPS spectrum analysis suggest that the surface layer of Ag/LSM/CFC has a higher oxidation environment than the bulk, which leads to the formation of more oxygen vacancies and results in a more disordered oxygen lattice. In the process of oxygen electrocatalysis, the presence of more oxygen vacancies and the existence of B-site cations in the form of truncated BO_5 octahedra on the surface of LSM are bound to accelerate the adsorption and charge transfer of oxygen-containing species to enhance the ORR catalytic activity of Ag/LSM/CFC [35, 36]; therefore it is reasonable to infer that the high ORR catalytic activity on the surface of LSM lies in its intrinsic structure.

The high-resolution XPS spectrum reveals that the C1s peak of CFC (Figure 2c) at 283.9 eV is associated with C-C bonds [37], and the peak at 282.6 eV suggests that it can be an electronic interaction between LSM and C [38]. The electronic interaction between LSM and C not only facilitates the transfer of electrons but also ensures the stability of the catalyst microstructure. In the Ag 3d high-resolution XPS spectra (Figure 2d), the two peaks appear at approximately 366.3 eV and 372.3 eV represent Ag 3d5/2 and Ag 3d3/2, respectively [25], which are from the silver oxide further confirming that the surface of silver is oxidized. To determine the valence state of Mn and the number of oxygen vacancies on the surface of LSM, the Mn 2p XPS spectra were also studied in detail, as shown in Figure 2e. There are two distinct peaks at 641 eV and 642.1 eV in the Mn 2p3/2 spectrum on the surface of LSM, which are related to Mn^{3+} and Mn^{4+}, respectively. The ratio of Mn^{4+}/Mn^{3+} is 0.632 according to the relative areas of the fitted subpeaks. The existence of Mn^{4+} on the surface of LSM also boosts the formation of high concentrations of oxygen vacancies and good oxygen ion conduction, thus confirming the inference obtained from the elemental content. Figure 2f shows the high-resolution XPS spectra of O 1s. The O 1s peaks at approximately 529.1 and 530 eV are attributed to the lattice oxygen (O_{latt}) and the adsorbed oxygen (O_{ads}), respectively. The peak at a binding energy of approximately 531 eV is associated with the oxygen vacancies (O_v) formed in surface of LSM [39-41]. The percentages of O_{latt}, O_{ads} and O_v are

14.9%, 47.9% and 37.2%, respectively, from the fitting results of the subpeaks. The large amount of absorbed oxygen on the surface of LSM will accelerate its ORR kinetics, and the plentiful oxygen vacancies will result in more active sites for catalytic reactions.

3.2 Electrocatalytic properties

Figure 3 presents the ORR catalytic properties of the Ag/CFC, LSM/CFC and Ag/LSM/CFC catalysts in oxygen-saturated 0.1 M KOH solution. The cyclic voltammetry (CV) curves of these three catalysts at a scan rate of 50 mV·s^{-1} are shown in Figure 3a. Figure 3b presents the linear sweep voltammetry (LSV) curves of these three catalysts at a scan rate of 5 mV·s^{-1}.

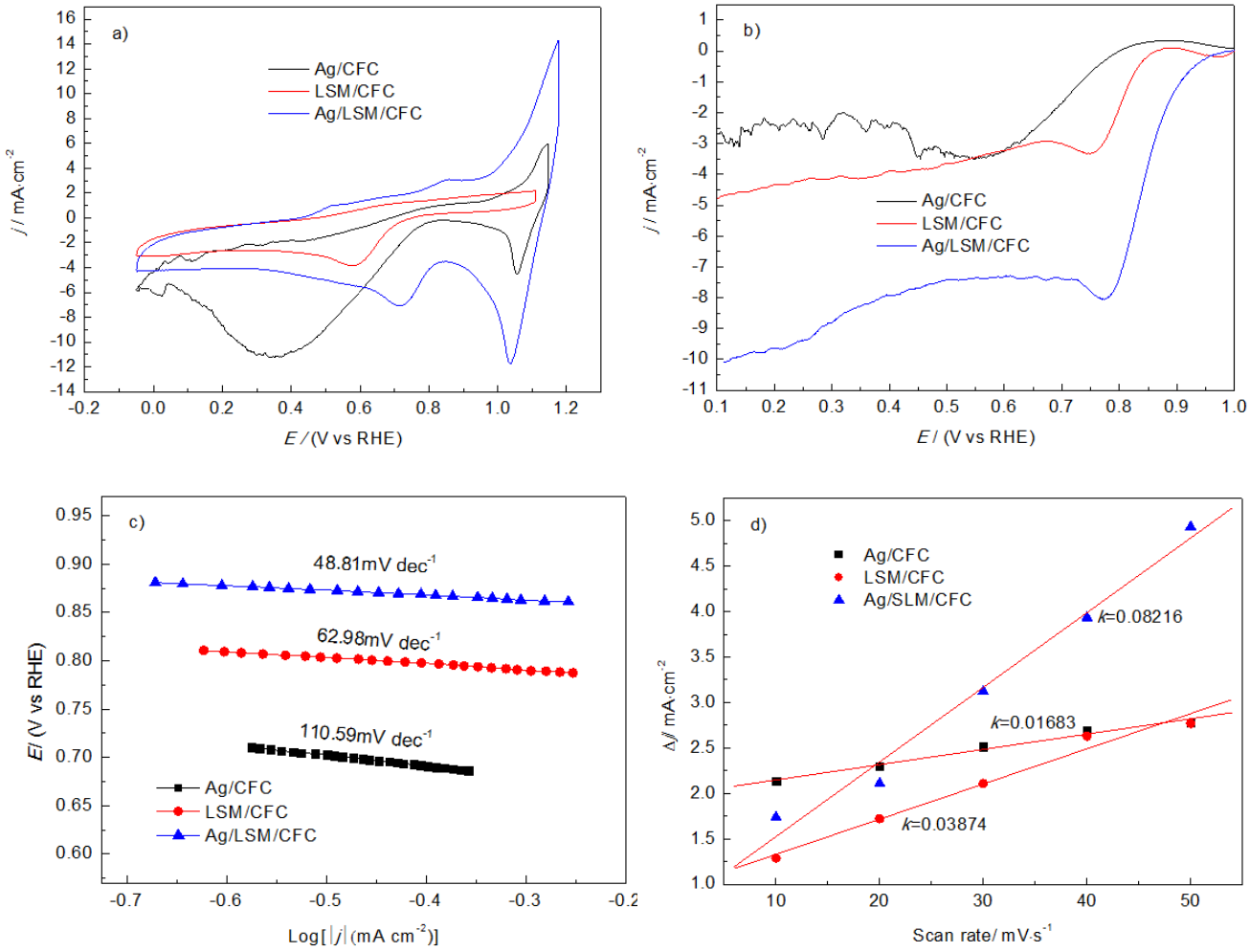

Figure 3. Comparison of ORR performance in O_2-saturated 0.1 M KOH solution for the Ag/CFC, LSM/CFC and Ag/LSM/CFC catalysts: (a) CV curves recorded at 50 mV·s^{-1}, (b) polarization curves with a scan rate of 5 mV·s^{-1}, (c) Tafel plots and (d) capacitive current densities ($\Delta j = j_a - j_c$, j_a and j_c are the current densities of the anode and cathode, respectively) of the middle potential as the function of the scanning rates.

The electrochemical parameters obtained from LSV are listed in Table 2. According to Figure 3a and b, LSM/CFC exhibits a cathodic ORR peak at 0.583 V and a half-wave potential at 0.788 V, whereas two cathodic ORR peaks in Ag/LSM/CFC appear at 0.72 V and 1.036 V, respectively. Ag/CFC presents a high cathodic peak at 1.055 V and a low half-wave potential at 0.694 V.

Table 2. Electrochemical parameters concerning the ORR and OER performance of the catalysts

catalysts	ORR			OER		E_{j10}- $E_{1/2}$
	E_{onset} (V)	$E_{1/2}$ (V)	J_{limit}/mA·cm^{-2}	E_{onset}/V	E_{j10} (V)	
Ag/CFC	0.798	0.694	-2.69	1.699	2.048	1.354
LSM/CFC	0.866	0.788	-4.86	1.679	1.898	1.11
Ag/LSM/CFC	0.99	0.833	-10.11	1.516	1.633	0.8

The higher cathode peak potential and half-wave potential of Ag/LSM/CFC compared to those of LSM/CFC reveal that the silver modification enhances the ORR catalytic activity of LSM/CFC. As can be seen from Figure 3b and Table 2, the ORR initial potential (E_{onset}) of the three catalysts increases from 0.798 V (Ag/CFC) to 0.99 V (Ag/LSM/CFC). The variation tendency of the half-wave potential ($E_{1/2}$) and the limiting current density (j_{limit}) is similar to that of E_{onset}. Ag/LSM/CFC has a more positive half-wave potential (0.833 V) and a larger j_{limit} (10.11 mA·cm^{-2}) than those of the other electrodes. The j_{limit} of Ag/LSM/CFC is more than two times that of LSM/CFC (4.86 mA·cm^{-2}) and is nearly four times that of Ag/CFC (2.69 mA·cm^{-2}). The comparison of the electrocatalytic activities of Ag/LSM/CFC with other representative $La_xSr_{1-x}MnO_{3-\delta}$ based ORR electrocatalysts reported in 0.1 M KOH solution are listed in Table 3,revealing the better ORR catalytic activity of Ag/LSM/CFC.

The ORR kinetics of these catalysts is evaluated by using Tafel curves, as shown in Figure 3c. The Tafel slopes of the Ag/CFC, LSM/CFC and Ag/LSM/CFC electrodes are obtained by fitting the linear part of the Tafel curves with the Tafel equation ($E = a + b\log|j|$). The slope of Ag/CFC is 110.59 mV·dec^{-1} and LSM/CFC is 62.98 mV·dec^{-1}, which are more than 2.26 and 1.28 times that of Ag/LSM/CFC (48.81 mV·dec^{-1}), respectively, suggesting the higher reaction rate and faster ORR kinetics of Ag/LSM/CFC.

Table 3. Comparison of the electrocatalytic activities of Ag/LSM with some representative $La_xSr_{1-x}MnO_{3-\delta}$ based ORR electrocatalysts reported in 0.1 M KOH

Catalysts	E_0 (V)	$E_{1/2}$ (V)	Tafel Slope (mV dec^{-1})	Reference
$La_{0.8}Sr_{0.2}MnO_{3-\delta}$	0.866	0.788	62.98	This work
Ag/ $La_{0.8}Sr_{0.2}MnO_{3-\delta}$	0.99	0.833	48.81	This work
$La_{0.9}Y_{0.1}MnO_{3-\delta}$	0.909	0.75	101	[42]
$(La_{0.7}Sr_{0.3})_{0.98}MnO_{3-\delta}$/C	0.903	0.588	92	[43]
$La_{0.8}Sr_{0.2}MnO_{3-\delta}$	-0.142 (*vs*.Ag/AgCl)	-0.316 (*vs*.Ag/AgCl)	NA	[44]
$La_{0.7}(Sr_{0.15}Pd_{0.15})MnO_{3-\delta}$	0.973	0.756	87	[30]
$La_{0.7}Sr_{0.3}MnO_{3-\delta}$	0.875	0.642	NA	[45]

$La_{0.7}Sr_{0.3}MnO_{3-\delta}$-$CeO_2$	0.881	0.666	NA	[45]
$(La_{0.8}Sr_{0.2})_{0.95}Mn_{0.9}Co_{0.1}O_{3-\delta}$	-0.09 (*vs*.Ag/AgCl)	NA	95	[31]
$(La_{0.8}Sr_{0.2})_{0.95}Mn_{0.95}Co_{0.05}O_{3-\delta}$	-0.09 (*vs*.Ag/AgCl)	NA	97	[31]
$La_{0.8}Sr_{0.2}MnO_{3-\delta}$	-0.1 (*vs*.Ag/AgCl)	NA	NA	[46]
$(La_{0.8}Sr_{0.2})_{0.95}Mn_{0.95}Ir_{0.05}O_{3-\delta}$	-0.05 (*vs*.Ag/AgCl)	NA	NA	[46]

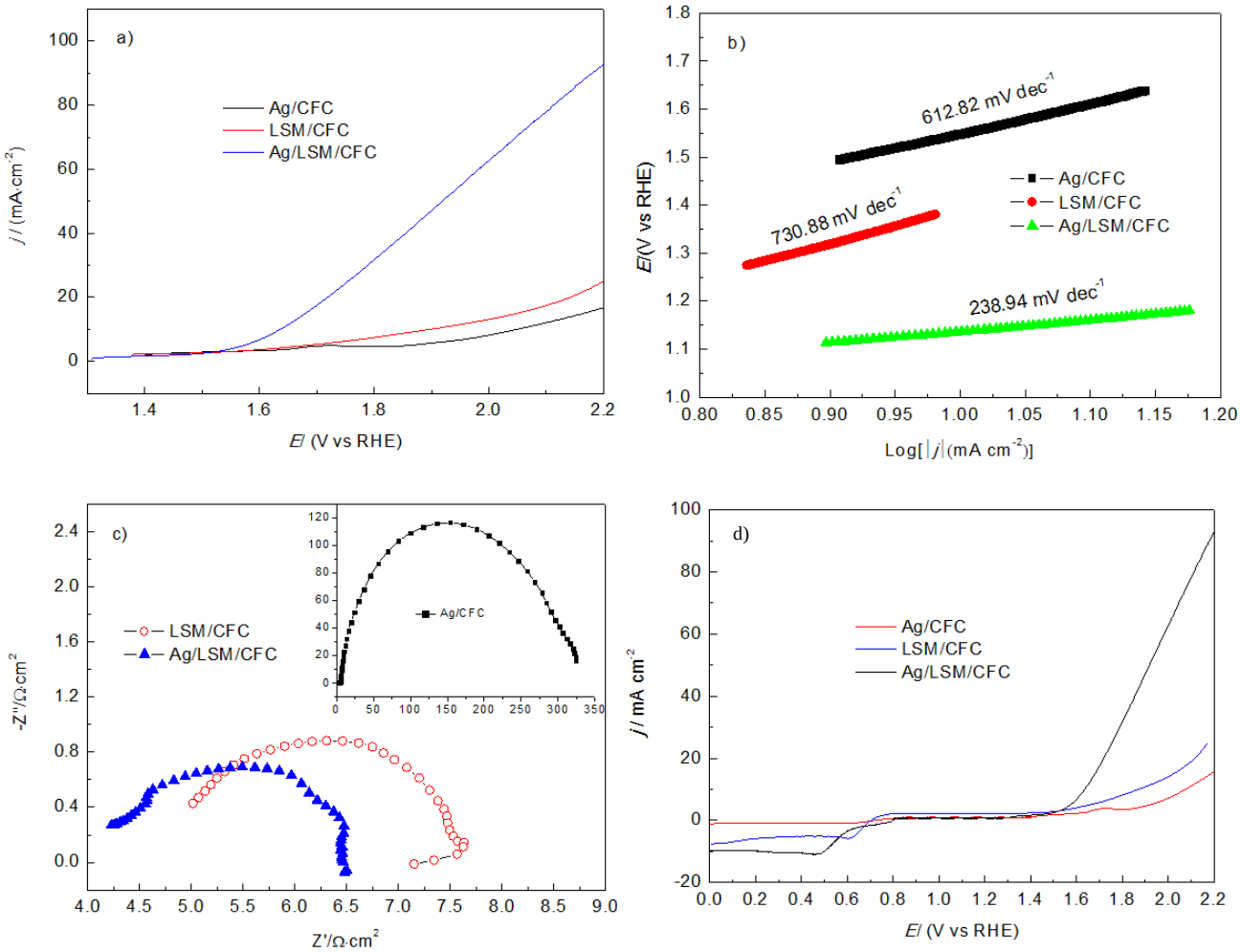

Figure 4. Comparison of OER performance in 0.1 M KOH solution for Ag/CFC, LSM/CFC and Ag/LSM/CFC catalysts: (a) polarization curves with a scan rate of 5 $mV \cdot s^{-1}$, (b) Tafel plots, (c) Nyquist plots of EIS spectra at 1.59 V *vs* RHE and (d) the overall polarization curves within the ORR and OER potential window.

The ORR kinetics of Ag/LSM/CFC is also faster than those of many other $La_xSr_{1-x}MnO_{3-\delta}$ based ORR electrocatalysts (Table 3). The electrochemical surface area (ECSA) values of the Ag/CFC, LSM/CFC and Ag/LSM/CFC catalysts were also measured to conduct an in-depth study of their ORR catalytic activities. After all, ECSA is one of the primary factors determining the catalytic activity of the ORR. Double layer capacitances (C_{dl}) determined by CV measurements are usually used to assess the

actual ECSA of the electrodes, as shown in Figure 3d, because the specific surface areas calculated by the BET method have difficulty accurately estimating ECSA. However, the linear slope of the capacitance current versus the scan rate determines the C_{dl} value of the catalysts, which are proportional to the ECSA. As can be seen from Figure 3d, the capacitance currents of these three catalysts have a linear relationship with the scan rate. Moreover, the calculated C_{dl} value (82.16 mF·cm^{-2}) of the Ag/LSM/CFC catalyst is the highest among these three catalysts, which is more than two fold that of LSM/CFC, revealing that the silver modification greatly increases its actual electrochemical surface area. Ag/CFC has the smallest electrochemical surface area of 16.83 mF·cm^{-2}, due to its relatively large silver particle size and less silver deposition, as observed by SEM.

In addition to the ORR catalytic activity, the oxygen evolution reaction (OER) activity of these catalysts was also evaluated. Figure 4a presents the LSV curves of Ag/CFC, LSM/CFC and Ag/LSM/CFC. Their corresponding onset potentials (E_{onset}) and the potentials at 10 mA cm^{-2} ($E_{10\ mA\ cm^{-2}}$) are listed in Table 2. This shows that the current density of Ag/LSM/CFC increases rapidly after E_{onset}. Ag/LSM/CFC demonstrates much higher OER performance than Ag/CFC and LSM/CFC with E_{onset} and $E_{10\ mA\ cm^{-2}}$ values of 1.516 V and 1.633 V, respectively. Whereas the current densities of Ag/CFC and LSM/CFC increase slowly with increasing potential, they present even higher values of E_{onset} and $E_{10\ mA\ cm^{-2}}$ compared to that of Ag/LSM/CFC. The OER catalytic activity was also examined by a Tafel curve analysis. Figure 4b shows the Tafel slopes of these three catalysts. Compared with LSM/CFC, Ag/CFC seems to have a relatively high Tafel slope (612.82 mV dec^{-1}); however, the synergy of silver and LSM greatly enhances the OER kinetics and exhibits a low Tafel slope of 238.94 mV dec^{-1}, demonstrating the good OER kinetics of Ag/LSM/CFC.

In addition, the surface OER kinetics of the catalysts were also examined by electrochemical impedance spectroscopy (EIS) analysis under the operating conditions, and their corresponding Nyquist plots are shown in Figure 4c. By fitting the EIS data, it can be confirmed that silver has an obvious effect on the reduction of solution resistance (R_Ω), and the R_Ω of LSM/CFC (5.0 Ω cm^2) is reduced to 4.18 Ω cm^2 with the silver modification. In contrast, the silver modification has little effect on the charge-transfer process. The charge-transfer resistance (R_{ct}) of LSM/CFC and Ag/LSM/CFC is close and much smaller than that of Ag/CFC. The small specific surface area and low catalyst content lead to Ag/CFC having a large R_{ct}. Figure 4d shows the overall polarization curves of Ag/CFC, LSM/CFC and Ag/LSM/CFC toward the ORR and OER in a potential range of 0-2.2 V. The potential differences ($\Delta E=E_{j10}-E_{1/2}$) between the ORR and OER curves were calculated and listed in Table 2 to evaluate the bifunctionality of the catalysts. E_{j10} is the OER potential at 10 mA cm^{-2} and $E_{1/2}$ is the half-wave potential for ORR. Clearly, Ag/LSM/CFC exhibits the best bifunctional oxygen electrocatalysis performance among these three catalysts with the smallest ΔE value of 0.8 V; furthermore, this value is comparable to recently reported values of superior bifunctional catalysts [42]. Although the synergistic effect between LSM and silver has greatly enhanced the ORR kinetics and ORR/OER reversibility of Ag/LSM/CFC, the slow OER kinetics of Ag/LSM/CFC will unavoidably inhibit its practical application in rechargeable metal-air batteries.

3.3 Flexible Al-air battery discharge performance

Several homebuilt Al-air batteries were fabricated with Ag/CFC, LSM/CFC and Ag/LSM/CFC as air cathodes to further inspect their ORR electrocatalytic performance in a real battery. Figure 5a presents the polarization curves and their corresponding power densities.

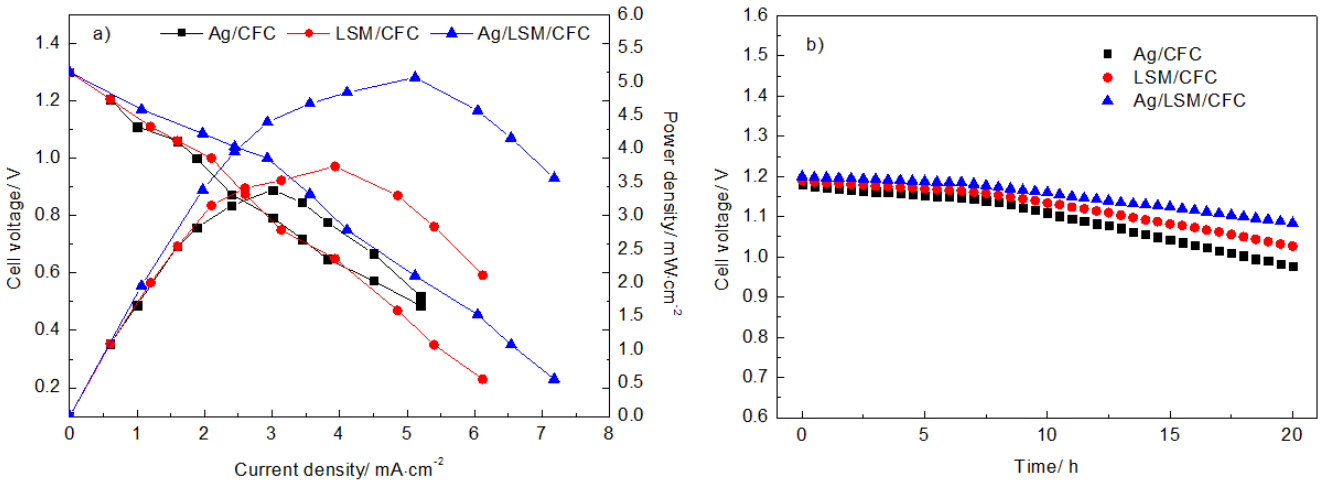

Figure 5. (a) Polarization curves and power density plots and (b) galvanostatic long-term stability tests at a current density of 5 mA·cm^{-2} for the flexible Al-air batteries with Ag/CFC, LSM/CFC and Ag/LSM/CFC as air electrodes.

Al-air batteries with Ag/CFC, LSM/CFC and Ag/LSM/CFC as the cathodes have roughly the same open circuit voltage (OCV) values of approximately 1.3 V, and their corresponding highest power densities are 3.02, 3.95 and 5.14 mW·cm^{-2}, respectively; the above values are comparable to the recently reported paper-based Al-air battery by Leung et al [8]. The discharge stability of each battery was also tested under a current density of 5 mA·cm^{-2}, as shown in Figure 5b. With Ag/LSM/CFC as the cathode, the cell voltages was reduced from 1.2 V to 1.09 V after 20 h of discharge, while for the batteries with Ag/CFC and LSM/CFC as the cathodes, the cell voltages decreased by 17.2% and 13.7%, respectively. Apparently, the silver-modified LSM/CFC air electrode has superior electrocatalytic activity and enhanced stability compared with Ag/CFC and LSM/CFC in a flexible Al-air battery.

4. CONCLUSIONS

In this work, an additive-free three-dimensional (3D) hierarchical catalyst (Ag/LSM/CFC) was designed as the cathode of a flexible Al-air battery. The electrochemical performance characterizations demonstrated that Ag/LSM/CFC had superior ORR catalytic activity and ORR/OER reversibility. The enhanced electrocatalysis effect resulted from the unique 3D hierarchical microstructure and the synergy between the silver and LSM. The silver modification not only reduced R_{ohm} and accelerated the ORR kinetics but also enlarged the ECSA of the Ag/LSM/CFC electrode. A flexible Al-air battery with

Ag/LSM/CFC as the air electrode exhibited a high power density and superior stability. Ag/LSM/CFC could be a possible ORR catalyst candidate for Al-air batteries and rechargeable metal-air batteries.

ACKNOWLEDGMENTS
This work was supported by the Opening Project of State Key Laboratory of Advanced Chemical Power Sources (Grant No. SKL-ACPS-C-09).

CONFLICT OF INTEREST
The authors declare no conflict of interest.

References

1. X. Cai, L. Lai, J. Lin and Z. Shen, *Mater. Horiz*., 4 (2017) 945.
2. P. Tan, B. Chen, H. Xu, H. Zhang, W. Cai, M. Ni, M. Liu and Z. Shao, *Energy Environ. Sci*., 10 (2017) 2056.
3. Y. Lin, H. Zhang, W. Deng, D. Zhang, N. Li, Q. Wu and C. He, *J. Power Sources,* 384 (2018) 278.
4. Z. Y. Xiong, C. I. Liao, W. H. Han and X. G. Wang, *Adv. Mater*., 27 (2015) 4469.
5. L. B. Liu, Y. Yu, C. Yan, K. Li and I. J. Zheng, *Nat. Commun*., 6 (2015) 7260.
6. S. Jung, J. Lee, T. Hyeon, M. Lee and D. H.Kim, *Adv. Mater*., 26 (2014) 6329.
7. S. K. Das, S. Mahapatra and H. Lahan, *J. Mater. Chem. A*, 5 (2017) 6347.
8. Z. Zhang, C. Zuo, Z. Liu, Y. Yu, Y. Zuo and Y. Song, *J. Power Sources*, 251 (2014) 470.
9. J. Li, Z. Zhou, K. Liu, F. Li, Z. Peng, Y. Tang and H. Wang, *J. Power Sources*, 34 (2017) 30.
10. M. Y. Oh, S. K. Park, H. K. Park, H. Kim, K. Kang, J. H. Kim, K. C. Roh and T. H. Shin, *ACS Appl. Energy Mater*., 1(2018) 5518.
11. T. V. Cleve, E. Gibara and S. Linic, *ChemCatChem*., 8 (2016) 256.
12. A. Zadick, L. Dubau, N. Sergent, G. Berthomé and M. Chatenet, *ACS Catal*., 5 (2015) 4819.
13. S. Cherevko, G.P. Keeley, S. Geiger, A.R. Zeradjanin, N. Hodnik, N. Kulyk and K.J.J. Mayrhofer, *ChemElectroChem*., 2 (2015) 1407.
14. C. J. Fu, K. N. Sun, N. Q. Zhang and D. R. Zhou, *Chem. J. Chinese U.*, 28 (2007) 1762.
15. H. H. Jiang and F. Zhang, *Int. J. Electrochem. Sci.*, 15 (2020) 959.
16. S. Jin, A.G. Hubert, Y. Naoaki, N. Haruyuki, B.G. John and Y. Shao-Horn, *Nat. Chem*., 3 (2011) 546.
17. J. Suntivich, H.A. Gasteiger, N. Yabuuchi and Y. Shao-Horn, *J. Electrochem. Soc*., 157 (2010) B1263.
18. R. Marcel, A.S. Kelsey, M. Shingo, T.H. Welsey, T. Ichiro and Y. Shao-Horn, *J. Am. Chem. Soc*., 136 (2014) 5229.
19. K.A. Stoerzinger, M. Risch, J. Suntivich, W. M. Lü, J.G. Zhou, M.D. Biegalski, H.M. Christon, A. Venkatesandeh and Y. Shao-Horn, *Energy Environ. Sci*., 6 (2013) 1582.
20. Y. Miyahara, K. Miyazaik, T. Fukutsuka and J. Abe, *J. Electrochem. Soc*., 161 (2014) F694.
21. Y. Liu, Q. Sun, W. Li, K.R. Adam, J. Li and X. Sun, *Green Energy Environ*., 2 (2017) 246.
22. Y. Zhu, W. Zhou and Z. Shao, *Small*, 13 (2017) 1.
23. Z. Wang, M. Li, C. Liang, L. Fan, J. Han and Y. Xiong, *RSC Adv*., 6 (2016) 69251.
24. S. Cai, M. Zheng, X. Lin, M. Lei, R. Yuan and Q. Dong, *ACS Catal*., 8 (2018) 7983.
25. Y. Chang, Y. Tian, S.W. Tsang and C. Yan, *Electrochim. Acta*, 174 (2015) 919.
26. J. Liu, W. Song, F. Wang and Y. Song, *J. Mater. Chem. A*, 2 (2014) 17477.
27. X. Wu, F. Chen, N. Zhang, A. Qaseem and R.L. Johnston, *J. Mater. Chem. A*, 4 (2016) 3527.
28. A. Qaseem, F.Y. Chen, X.Q. Wu and R.L. Johnston, *Catal. Sci. Technol*., 6 (2016) 3317.
29. J.J. Xu, D. Xu, H.G. Wang, L.L. Zhang and X.B. Zhang, *Angew Chem. Int. Ed.*, 52 (2013) 3887.
30. Y. Xue, S. Sun, Q. Wang, H. Miao, S. Li and Z. Liu, *Electrochim. Acta*, 230 (2017) 418.

31. W. Xu, L. Yan, L. Teich, S. Liaw, M. Zhou and H. Luo, *Electrochim. Acta*, 273 (2018) 80.
32. E. Symianakis, D. Malko, E. Ahmad, A.S. Mamede, J.E. Paul, N. Harrison and A. Kucernak, *J. Phys. Chem. C*, 119 (2015) 12209.
33. E.J. Crumlin, E. Mutoro, Z. Liu, M.E. Grass, M.D. Biegalski, Y.L. Lee, D. Morgan, H.M. Christen, H. Bluhm and Y. Shao-Horn, *Energy Environ. Sci*., 5 (2012) 6081.
34. D. Mierualdt, S. Mildner, R. Arrigo, A. Knop-Gericke, E. Franke, A. Blumenstein, J. Hoffmann and C. Joose, *Catalysts*, 4 (2014) 129.
35. E.A. Ahmad, V. Tileli, D. Kramer, G. Mallia, K.A. Stroerzinger, Y. Shao-Horn, A.R. Kucernak and N.M. Harrison, *J. Phys. Chem. C*, 119 (2015) 16804.
36. R.P. Fang, S.Y. Zhao, P.X. Hou, M. Cheng, S.G. Wang, H.M. Cheng, C. Liu and F. Li, *Adv. Mater*., 28 (2016) 3374.
37. K. Nishio, S. Molla, T. Okugaki, S. Nakanishi, L. Nitta and Y. Kotani, *J. Power Sources,* 298 (2015) 236.
38. N.A. Merino, B.P. Barbero, P. Eloy and L.E. Cadús, *Appl. Surf. Sci*., 253 (2006) 1489.
39. S. Ponce, M.A. Peña, J.L.G. Fieero, *Appl. Catal. B Environ*., 24 (2000) 193.
40. D.Y. Yoon, E. Lim, Y.J. Kim, J.H. Kim, T. Ryu, S. Lee, B.K. Cho, I.S. Nam, J.W. Choung and S. Yoo, *J. Catal*., 319 (2014) 182.
41. Y.F. Wang, H. Kwok, W.D. Pan, H.M. Zhang and D.Y.C. Leung, *J. Power Sources*, 414 (2019) 278.
42. H. Miao, Z. Wang, Q. Wang, S. Sun, Y. Xue, F. Wang, J. Zhao, Z. Liu and J. Yuan, *Energy*, 154 (2018) 561.
43. Y. Xue, H. Miao, S. Sun, Q. Wang, S. Li and Z. Liu, *J. Power Sources*, 342 (2017) 192.
44. F. Lu, Y. Wang, C. Jin, F. Li, R. Yang and F. Chen, *J. Power Sources*, 293 (2015) 726.
45. Y. Xue, H. Huang, H. Miao, S. Sun, Q. Wang, S. Li and Z. Liu, *J. Power Sources*, 358 (2017) 50.
46. L. Yan, Y. Lin, X. Yu, W. Xu, T. Salas, H. Smallidge, M. Zhou and H. Luo, *ACS Appl. Mater. Interfaces*, 9 (2017) 23820.
47. X. F. Lu, Y. Chen, S. B. Wang, S.Y. Gao and X. W. Luo, *Adv. Mat*., 31 (2019) 1.

© 2020 The Authors. Published by ESG (www.electrochemsci.org). This article is an open access article distributed under the terms and conditions of the Creative Commons Attribution license (http://creativecommons.org/licenses/by/4.0/).